Biomacromolecules

pubs.acs.org/Biomac

Article

Glycosylated Polyhydroxyproline Is a Potent Antifreeze Molecule

Published as part of Biomacromolecules virtual special issue "Peptide Materials".

Thomas J. McPartlon, Charles T. Osborne, and Jessica R. Kramer*

Cite This: *Biomacromolecules* 2024, 25, 3325−3334

Read Online

ACCESS | Metrics & More | Article Recommendations | Supporting Information

ABSTRACT: Molecules that inhibit the growth of ice crystals are highly desirable for applications in building materials, foods, and agriculture. Antifreezes are particularly essential in biomedicine for tissue banking, yet molecules currently in use have known toxic effects. Antifreeze glycoproteins have evolved naturally in polar fish species living in subzero climates, but practical issues with collection and purification have limited their commercial use. Here, we present a synthetic strategy using polymerization of amino acid *N*-carboxyanhydrides to produce polypeptide mimics of these potent natural antifreeze proteins. We investigated a set of mimics with varied structural properties and identified a glycopolypeptide with potent ice recrystallization inhibition properties. We optimized for molecular weight, characterized their conformations, and verified their cytocompatibility in a human cell line. Overall, we present a material that will have broad applications as a biocompatible antifreeze.

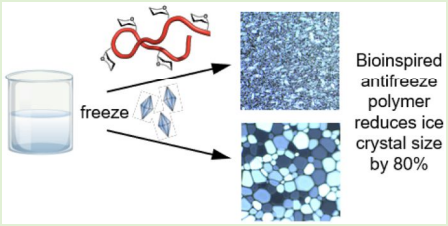

INTRODUCTION

Worldwide, animal species have adapted strategies to survive subfreezing temperatures.[1−4] A particularly interesting example is the convergent evolution of antifreeze glycoproteins[5] (AFGPs) in polar fish, which are the most potent ice-binding molecules discovered to date.[6,7] Protein binding to embryonic ice crystals modifies their shape and growth rate, resulting in small crystals, lower plasma freezing points, and prevention of mechanical damage to cells and tissues by large crystals.

There is a broad demand for antifreeze molecules for applications in food technology, agriculture, fisheries, coatings, building materials, and the petroleum industry.[8,9] Additionally, there is a great need for nontoxic ice-recrystallization inhibitors (IRI) to improve post-thaw tissue viability and function in biomedical cryopreservation.[10,11] For decades, AFGPs have been explored in the cryopreservation of tissues and even whole organs[10−13] and have even been utilized as texture-improving ice cream additives.[14] However, the expense and impracticality of harvesting these specialized proteins from polar fish have limited widespread use. Dimethyl sulfoxide and glycerol are still standard cellular cryoprotectants despite well-known toxic effects.[15,16] AFGPs have the potential to revolutionize biomedical cryopreservation by replacing toxic CPAs or acting as an effect-boosting additive in CPA mixtures. However, lack of consensus on optimal cryopreservation conditions and lack of mechanistic details hinder their widespread use.[10,12,17−19]

A wide variety of short peptides and polymer alternatives have been explored as AFGP mimics, but none have achieved comparable potency to AFGPs and require orders of magnitude higher concentration for observable effects.[9,20−37] Depending on protein molecular weight, native AFGPs can fully inhibit ice crystal growth at concentrations from 0.022 to 0.22 μg/mL, with longer chains displaying higher activity at lower concentrations.[6,38] By contrast, 1−20 mg/mL poly(vinyl alcohol) (PVA)[29,39,40] or 5−40 mg/mL proline polymers/oligomers[26,28] is needed for IRI activity and 100- to 1000-fold higher concentrations were used in cell experiments. As with native AFGPs, the potency was dependent upon the material's chain length.

Our lab recently reported a breakthrough in the scalable preparation of synthetic AFGPs that are based on the exact chemical motifs in the native protein structure.[41] AFGP molecular structure is relatively simple, consisting of a highly conserved Ala-Ala-Thr repeat, where Thr is glycosylated with the disaccharide αGal(1 → 3)αGalNAc (Figure 1).[42] Polyprotein genes encode for isoforms with molecular weights from 2.6 to 33.7 kDa, classified as AFGP8−AFGP1, which correlates to 12−150 residues.[5] Due to steric and hydrogen bonding effects from the Thr methyl and bulky sugar groups, AFGPs adopt an extended structure similar to a polyproline type II (PPII) helix.[41,43−45]

For decades, the molecular mechanisms of AFGP-ice binding have been debated. It has generally been accepted that after adsorption of the glycoprotein to an embryonic ice crystal, approaching liquid water molecules become disordered, resulting in inhibited crystal growth, ice shaping, and

Received: December 31, 2023
Revised: May 9, 2024
Accepted: May 10, 2024
Published: May 22, 2024

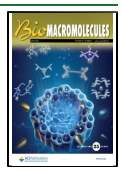

https://doi.org/10.1021/acs.biomac.3c01462
Biomacromolecules 2024, 25, 3325−3334

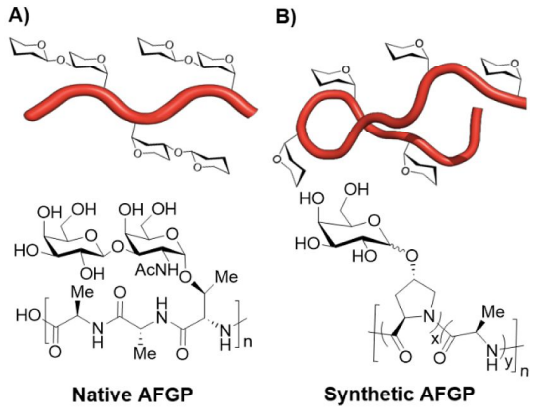

Figure 1. Chemical structure and cartoon representation of (A) native AFGPs as compared to (B) our synthetic mimics based on statistical copolymers of galactosylated-Pro and Ala.

lowered melting point.[46−48] However, until recently, the roles of hydrophobic Ala versus hydrophilic sugars have been unclear.[41,49−54] This is in part due to the lack of access to sufficient quantities of AFGPs for experimental purposes and also since native AFGPs can only be isolated in heterogeneous mixtures rendering structure−function studies difficult. To date, these glycoproteins have resisted recombinant production.[8,9,55]

Our recently described method for the preparation of synthetic AFGPs, based on amino acid *N*-carboxyanhydride (NCA) polymerization, allows precise tuning of glycopolypeptide molecular characteristics.[41] Variation of the ratios of Ala to glycosylated Thr provided key experimental evidence that Ala is the driver of ice binding rather than the disaccharide-Thr residue. Reduction in Ala content resulted in reduced antifreeze activity.[41] The disaccharide could even be truncated to a variety of monosaccharide structures without a loss of IRI activity. These data corroborated molecular dynamics models of a 14-residue AFGP. The model predicted that Ala is crucial for IRI activity and that the residue's methyl groups nest into ice-surface cavities, driven by the entropy of dehydration.[49] The simulations also suggested that AFGP's extended PPII structures play a role in antifreeze activity.

Substitution of Pro in the Ala-Ala-Thr repeat has been observed in Antarctic fish.[5] PolyPro itself has been explored as a simplified antifreeze polymer.[26,30] PolyPro was found to exhibit length-dependent ice-binding and IRI activity. However, concentrations 10−40× of that of native or synthetic AFGPs were required.

Considering our recent data that Ala plays a dominant role in ice-binding, we wondered if the disaccharide-Thr could be substituted for simpler PPII-driving residues. The disaccharide structure requires lengthy syntheses and advanced skills in carbohydrate chemistry, and Thr requires harsher NCA cyclization conditions than many other amino acids due to steric hindrance by the methyl group and potential formation of the 2-oxazolidinone side product.[45] Therefore, we investigated copolypeptides composed of Ala and various Pro derivatives. Here, we report that galactosylated hydroxyproline (GalHyp) is a suitable substitute for the disaccharide-Thr residue and enables facile preparation of potent synthetic AFGP mimics (Figure 1).

EXPERIMENTAL SECTION

Materials and Instrumentation. Reactions were conducted under an inert atmosphere of N_2 and with oven-dried glassware and anhydrous solvents, unless otherwise stated. Deionized water (18 MΩ cm) was obtained by passing in-house deionized water through a Thermo Scientific MicroPure UV/UF purification unit. Infrared spectra were recorded on a Bruker Alpha ATR-FTIR spectrophotometer. For peracetylated polymers, tandem size exclusion chromatography/refractive index (SEC/MALS/RI) was performed on an Agilent 1260 Infinity liquid chromatograph pump equipped with a Wyatt DAWN HELEOS-II light scattering (LS) and Wyatt Optilab T-rEX refractive index (RI) detectors. Separations were achieved using 10^5, 10^4, and 10^3 Å Phenomenex Phenogel 5 μm columns using 0.10 M LiBr in DMF as the eluent at 60 °C. For aqueous GPC samples using deacetylated polymers, samples were analyzed on an Agilent 1260 Infinity equipped with UV, RI, and Wyatt miniDawn TREOS for light scattering. Samples dissolved in PBS at 3 mg/mL and were filtered via a 0.2 μm PTFE syringe filter. The eluent was DPBS without Ca & Mg, and the column utilized was Agilent AQ Gel−OH 30 <100−60,000> Da. The injection volume was 100 μL with a flow rate 1 mL/min. The degree of polymerization was also determined by ^{1}H NMR of poly(ethylene glycol) (PEG) end-capped polymers. CD measurements of the polypeptide solutions were recorded in quartz cells with a path length of 0.1 cm, on a JASCO J-1500 CD spectrophotometer. ^{1}H and ^{13}C NMR spectra were recorded on a Varian Mercury spectrometer (400 MHz) or an Agilent DirectDrive spectrometer (500 MHz) and are reported relative to a deuterated solvent.

Preparation of NCAs. Pro and AcO-Pro NCAs were prepared according to a previous publication.[56] The cyclization of Boc-GalOAc$_4$Hyp was completed similarly. The Boc-GalOAc$_4$Hyp (0.66 g, 1 equiv) was dissolved in anhydrous THF (11.76 mL, 0.1 M). Triphosgene (0.175 g, 0.5 equiv) was added and the solution was cooled to 0 °C. Epichlorohydrin (0.46 mL, 5 equiv) was added to the solution followed by dropwise addition of distilled TEA (0.0445 mL, 1.1 equiv). The reaction was stirred for 24 h, and the reaction progress was monitored by ATR-FTIR. After 24 h, the reaction was filtered through cotton to remove TEA-HCl salts. The reaction solution was evaporated under reduced pressure. The evaporate was sequestered in a tandem solvent trap system cooled by liquid N_2. The traps were immediately quenched with ammonium hydroxide. The crude product was purified using anhydrous silica chromatography[57] with 5%−15% THF in DCM. The collected fractions were analyzed by ATR-FTIR. NCA-containing fractions were combined, resulting in 0.41 g of white crystalline solid (73% yield).

General Method for Polymerization of NCAs to Prepare Homopolymers and Statistical Copolymers. All polymerizations were performed in a N_2-filled glovebox. NCAs were dissolved in anhydrous THF at 50 mg/mL in a vial or a bomb tube. To the NCA solution, a 30 mg/mL solution of $(PMe_3)_4Co$ or preinitiated Ni complex in THF was added.[56,58] PolyPro homopolymer was prepared using hexylamine as previously described.[59] The NCA:initiator ratio varied, yielding different-length polypeptides. The vials were left in the glovebox at ambient temperature, and the bomb tubes were removed from the glovebox and heated at 50 °C for 5−72 h. The reaction progress was monitored by attenuated total

https://doi.org/10.1021/acs.biomac.3c01462
Biomacromolecules 2024, 25, 3325−3334

reflectance Fourier transform infrared spectroscopy (ATR-FTIR). Upon completion, a portion of the polypeptides was removed for molecular weight analysis by size exclusion chromatography coupled to multiangle light scattering and refractive index detectors (SEC/MALS/RI) or end-capping and ^{1}H NMR.[56,59−61] Representative data can be found in the Supporting Information.

General Method for Deacetylation of AcO-Containing Copolymers. Polymer was suspended in 0.25 M K_2CO_3 in a 1:1 MeOH:H_2O mixture and stirred overnight. The solution was transferred to a 1 kDa spin filter and concentrated at 4000*g* for 20 min. The concentrate was diluted three times with Milli-Q water and spin-filtered at 4000*g* for 20 min each time. The concentrate was recovered, frozen, and lyophilized. Samples can also be dialyzed against Milli-Q water in 2000 MWCO dialysis tubing.

General Method for Observing Dynamic Ice Shaping.[41,62] To observe dynamic ice shaping, 10 μL of solution containing polypeptide in 1X PBS was placed on a microscope slide and sandwiched between a coverslip. The stage was rapidly cooled at a rate of 10 °C/min to −30 °C to freeze the polymer solution. The stage was then slowly warmed to −2.5 °C at a rate of 8 °C/min. Then, the stage was warmed to −1.8 °C at a rate of 0.5 °C/min. The stage temperature was then increased at a rate of 0.05 °C/min to −1.5 to −1 °C depending on the polypeptide solution used to isolate individual crystals. The stage was then cooled at 0.02 °C/min to −2 to −1.5 °C to observe dynamic ice shaping. The stage was then toggled between melting and freezing rates to observe the ice crystal change as the temperature was increased and then decreased. Images of the single crystals were taken as the temperature was decreased to observe ice crystal growth.

General Method for Cooling Splat Assays.[41,62] To make the ice wafer, 10 μL of solution containing polypeptide in PBS was dropped from 2 m through a PVC pipe onto a precooled slide using a micropipette. The slide was cooled on an aluminum block and rested in a bed of dry ice. The slide containing the ice splat was quickly moved to the temperature-controlled stage (Linkam LTS120, WCP, and T96 controller) precooled to −6.4 °C. The stage chamber was purged with N_2 to prevent condensation from growing on the ice splat. The ice splat was annealed for 40 min and images of the ice crystals were recorded at 0, 20, and 40 min using cross-polarizers (MOTICAM S3, MOTIC BA310E LED Trinocular) to observe ice recrystallization inhibition. Our highly quantitative method for determining mean grain size (MGS) and IRI activity is as follows. For every sample, three images were taken of different areas of the ice wafer. Image processing software (ImageJ (Fiji)) was used to determine individual grain size for larger crystals, or for samples with very high IRI and crystal sizes too small to be accurately determined by the software, crystals were sized manually. Statistical analyses showed that 150 μm × 150 μm regions of the images resulted in an MGS that is representative of the entire population in the image. We randomly selected regions of this size in each of 3 separate images to analyze. For samples that resulted in little to no IRI activity, 75 crystals were analyzed moving radially outward from a randomly selected point. In all cases, from this analysis of the three separate images, the ice crystal areas were averaged. The average and standard deviation of the three images are presented for each experiment and statistical significance was determined with a one-way ANOVA and post hoc Tukey tests, where ns indicates not significant, * indicates $p < 0.05$, and ** indicates $p < 0.01$.

General Method for Determining Cell Viability with a CCK8 Assay. HEK 293 cells were plated at a density of 10,000 cells/well in a 96-well plate. The cells were incubated at 37 °C in 5% CO_2 for 24 h to allow the cells to adhere to the plate. The cells were then treated with polymer dissolved in complete media (DMEM with 10% FBS supplemented with 1% penicillin-streptomycin and 1% L-glutamine) for a final polymer concentration of 0.02, 0.2, and 2.0 mg/mL. Additionally, other wells of cells are treated with 100-X Triton to kill cells for a positive control or media to serve a negative control. The treated cells were again incubated at 37 °C in 5% CO2 for 24 h. The cells were then dosed with 10 μL of CCK-8 solution (Dojindo) and incubated at 37 °C in 5% CO_2 for 3 h. The absorbance at 450 nm of the treated cells was measured after the 3 h incubation using a BioTek Synergy HTK multimode reader.

RESULTS

Antifreeze Polymer Design and Preparation. We prepared synthetic antifreeze glycoproteins via NCA polymerization. NCA polymerization is an attractive route to obtain polypeptides since the method is rapid, high yielding, scalable, and allows precise tuning of chain length up to high molecular weights.[45,61,63] Compared to solid-phase peptide synthesis, substantially higher molecular weights can be achieved, which has been shown to dramatically improve activity in both natural and synthetic AFGPs.[7,41,54,64,65] The method is much more scalable than recombinant protein production methods, and while recombinant nonglycosylated AFPs have been achieved, AFGPs have so far resisted all efforts.[8,9,55]

GalHyp was prepared in one step by coupling of commercially available peracetylated galactose and *N*-carbobenzyloxy-hydroxyproline-*O*-benzyl using boron trifluoride etherate as a Lewis acid (Scheme 1). The conjugate was

Scheme 1. Preparation of Galactose-Hydroxyproline Conjugates and Conversion to NCA Monomers

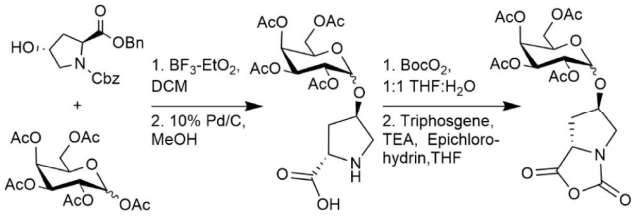

isolated as a mixture of 1:1 α/β anomers that were not separated. Amino acid-protecting groups were quantitatively removed by hydrogenolysis over palladium on carbon. Based on the prior work of our own lab and others, we formed GalHyp NCA using conditions optimized for Pro NCA cyclization via *t*-butoxycarbonyl-Pro with triphosgene and triethylamine. GalHyp NCA was obtained in excellent yield after purification by anhydrous flash column chromatography on dry silica in a fume hood.[2] Ala NCA was prepared according to published methods. Since polyPro and densely hydroxylated poly(vinyl alcohol) have also been explored as antifreeze polymers, we prepared Pro NCA and AcOHyp NCAs in order to examine polypeptides structurally related to GalHyp but that vary in hydroxyl density and potentially conformation.

https://doi.org/10.1021/acs.biomac.3c01462
Biomacromolecules 2024, 25, 3325−3334

NCA polymerization was initiated using $(PMe_3)_4Co$ for polypeptides containing Ala or with Ni-complexes for polypeptides containing only Pro-based structures since these complexes bypass the need for the NCA nitrogen proton (Scheme 2, see the Supporting Information).[3] Degrees of

Scheme 2. Preparation of Antifreeze Polymer Panel by NCA Polymerization[a]

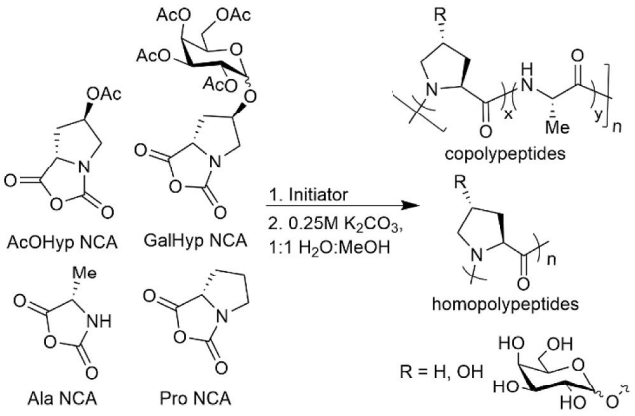

[a]$(PMe_3)_4Co$ or Ni-amido amidate complexes were utilized to initiate polymerization.

polymerization were readily tuned by altering the monomer/initiator ratios, and amino acid compositions were tuned via the NCA feed ratios. Polymer yields were quantitative and chain lengths were determined by end-group analysis as previously described[56,59−61] or by SEC/MALS/RI. See Table 1

Table 1. Representative Polymerization Data

polypeptide	M_n[a]	M_n[b]	DP[f]	Đ[g]
$(GalHyp_{0.33}\text{-}s\text{-}Ala_{0.66})_n$	8,643	6,758[c,e]	49	1.11[c]
$(GalHyp_{0.33}\text{-}s\text{-}Ala_{0.66})_n$	12,783	9,734[c,e]	70	1.24[c]
$(GalHyp_{0.33}\text{-}s\text{-}Ala_{0.66})_n$	16,923	11,520[c,e]	83	1.25[c]
$((GalOAc_4)_{0.25}\text{-}s\text{-}BnE_{0.75})_n$	41,610	30,080[d,e]	109	1.29[d]
$(Hyp_{0.33}\text{-}s\text{-}Ala_{0.66})_n$	12,930	13,113[e]	155	-

[a]Theoretical number-average molecular weight, M_n. [b]Observed M_n as determined by [c]SEC/MALS/RI in DPBS for deacetylated, free hydroxyl structures, or [d]SEC/MALS/RI in DMF with 0.1 M LiBr for peracetylated structures, or [e]^{1}H NMR end-group analysis as described in prior publications.[56,59−61] [f]Observed degree of polymerization, DP. [g]Polymer dispersity, Đ, as determined by SEC/MALS/RI as described in [c] and [d] or for the sample noted with (−), the dispersity could not be determined due to poor solubility in DMF and DPBS.

for representative polymer data, and the SI for additional data and experimental methodology. Glycan acetate-protecting groups were quantitatively removed after polymerization by treatment with K_2CO_3 in methanol:water.

Since polyPro is reported to have IRI activity, we prepared Pro homopolymers along with copolymers of varied GalHyp densities up to 100% GalHyp. Since polyhydroxylated PVA has also shown IRI activity, we prepared polyHyp from AcOPro NCA where the acetate groups were removed postpolymerization as previously described. We also prepared Hyp:Ala 1:2 to compare the effects of a single vs the four hydroxyls of GalHyp:Ala 1:2. For comparison of these polymers of varied amino acid compositions, chains were prepared at a similar length of ca. 100 residues (see Table S1). All samples were purified by dialysis against Milli-Q water.

Antifreeze Activity Assays. Native AFGPs bind irreversibly to embryonic ice crystals, inhibiting prism-face growth and influencing the macroscopic crystal shape and size (Figure 2, top left panel). This action results in an overall reduction in crystal mean grain size (MGS), i.e., IRI, and shaping of single crystals into characteristic hexagonal and bipyramidal structures.[52] To quantitate MGS and observe crystal shaping, we used cryostage microscopy and cooling splat assays.[7,41,62] Images were collected of the ice wafers at time zero and after 40 min of ice crystal growth. Particle size was quantified from 3 separate ice crystal images, 150 μm × 150 μm regions with a minimum of 75 crystals analyzed, and using image analysis software or manual sizing of crystals too small for software recognition. The average and standard deviation are presented for each experiment, and statistical significance was determined with a one-way ANOVA and post hoc Tukey test. Activities for our various polypeptides in PBS were compared to PBS alone.

IRI activity for the various (co)polypeptide structures is shown in Figure 2. At identical solution concentrations of 1 mg/mL in PBS, the 40 min MGS values for Pro_{100}, Hyp_{75}, and $GalHyp_{103}$ were not statistically different from PBS alone. However, the 40 min MGS for ice crystals formed in the presence of 1 mg/mL $(GalHyp_{0.33}\text{-}s\text{-}Ala_{0.66})_{103}$ was reduced by 61% from that of PBS alone (from ca. 4052 to 1588 μm^2). Clearly, Ala residues play a major role in IRI activity since the GalHyp homopolymer showed no discernible activity. We also attempted to collect IRI data for the copolypeptide $(Hyp_{0.33}\text{-}s\text{-}Ala_{0.66})_{100}$, but the sample had very poor aqueous solubility. Centrifugation revealed an insoluble portion totaling 50% of the mass. We measured the IRI activity of the soluble portion, which was relatively minor (Figures S6 and S9). Preparation of $(Pro_{0.33}\text{-}s\text{-}Ala_{0.66})_{100}$ yielded a material that was entirely insoluble in water. We also examined a higher molecular weight Hyp_{200} and though activity was slightly increased from that of the 75mer (Figures S10 and S11), the IRI effects were poor compared to those of the GalHyp:Ala copolymer. Clearly, the biomimetic glycosylated copolymer with native Ala content was the most promising antifreeze polymer candidate.

Since length-dependent function has been clearly established in native AFGPs, as well as in our prior disaccharide-Thr-based mimics, we prepared GalHyp-containing chains from 30−300 residues and with the native content of 66% Ala. Short chains of 30 residues had no statistical difference in MGS from that of PBS alone, indicating that this length is not sufficient for antifreeze activity (Figure 3C,D,J). Chains of 60 and 100 residues offered a reduction in ice crystal MGS similar to that of the common cryoprotectant DMSO (Figure 3B,E,F,J). A further 37% increase in IRI activity was observed with the increase in chain length from 100 to 150 residues, as evidenced by the reduction in MGS (Figure 3F,G,J). The effect plateaued, however, and further increasing the chain length to 225 or 300 residues did not result in any statistically significant increase in IRI activity (Figure 3G−J). The 150, 225, and 300 mers all offered a remarkable ca. 80% reduction in MGS. Examination of the 150 mer at varied concentrations indicated the effect is indeed concentration-dependent (Figure 3K). It is notable that our GalHyp:Ala copolymers of $n > 150$ residues achieved greater IRI activity (80% reduction vs 70% reduction in MGS) at 50-fold lower concentration than for 8-residue proline oligomers,[28] 5-fold lower than for proline polymers of a similar MW,[26] and similar to that of high MW

https://doi.org/10.1021/acs.biomac.3c01462
Biomacromolecules 2024, 25, 3325−3334

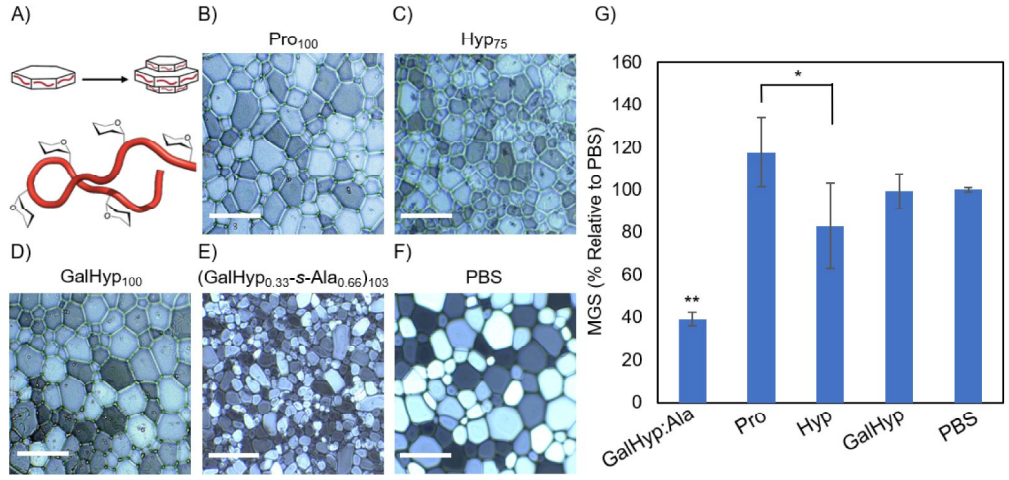

Figure 2. (A–F) IRI activity of various proline-based homo- and copolypeptide structures as compared to PBS alone. All samples were prepared at 1 mg/mL in PBS and ice crystals were imaged after 40 min of growth. Chain lengths were $(GalHyp_{0.33}\text{-}s\text{-}Ala_{0.66})_{103}$, Pro_{100}, Hyp_{75}, and $GalHyp_{100}$. Scale bars are 200 μm. (G) Quantified IRI data as MGS relative to PBS; mean and standard deviation, * indicates $p < 0.01$.

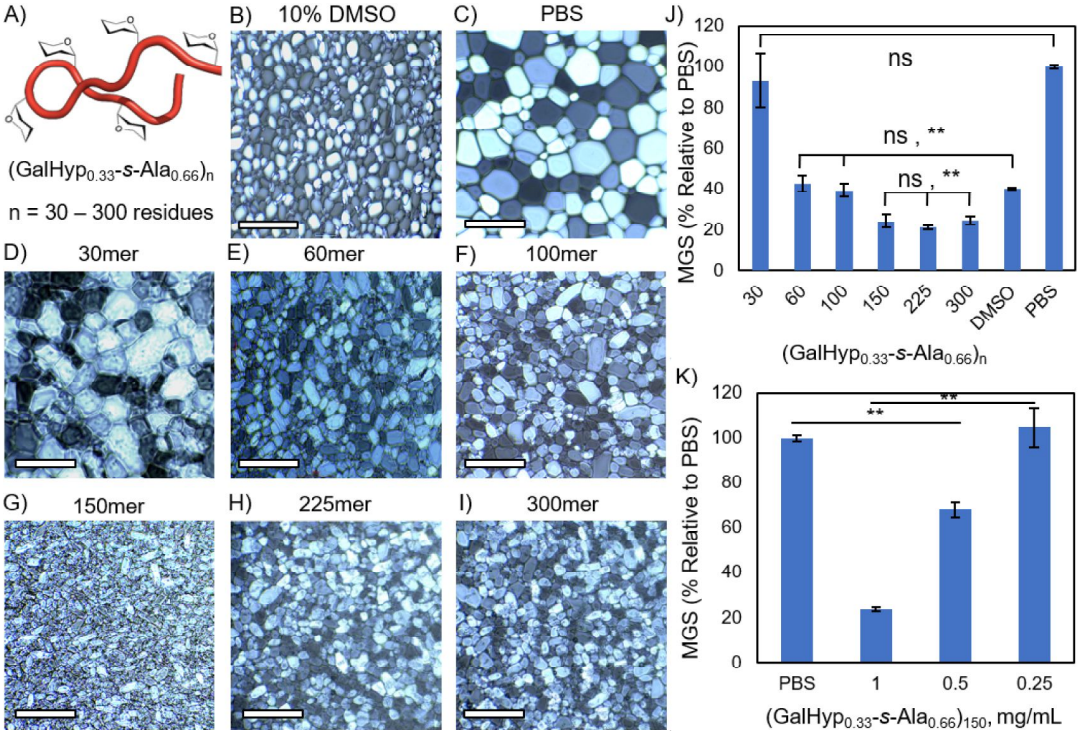

Figure 3. (A–I) IRI activity of $(GalHyp_{0.66}\text{-}s\text{-}Ala_{0.33})_n$ glycopolypeptides of varied chain lengths as compared to PBS alone or 10% DMSO in PBS. All glycopolypeptide samples were prepared at 1 mg/mL in PBS and ice crystals were imaged after 40 min of growth. Scale bar is 200 μm. (J) Quantified IRI data as MGS relative to PBS for varied chain lengths, 10% DMSO, or PBS; mean and standard deviation, * indicates $p < 0.01$. (K) Quantified IRI data for $(GalHyp_{0.66}\text{-}s\text{-}Ala_{0.33})_{150}$ at varied concentrations as compared to PBS; mean and standard deviation, * indicates $p < 0.01$.

PVA.[62] Additional imaging data at varied time points and videos of crystal growth are supplied in the SI to show the crystal growth rate for representative samples.

We also examined the ice-shaping properties of the $(GalHyp_{0.33}\text{-}s\text{-}Ala_{0.66})_n$ polymers since hexagonal shaping has been linked to ice-binding and IRI activity and since antifreeze materials resulting in spicular crystals that can cause cellular damage are not optimal. It is generally accepted that ice-shaping occurs after adsorption of the glycoprotein to specific crystal faces in embryonic ice, therefore inhibiting addition of new water molecules to that face and limiting crystal growth to specific planes.[46−48] Inhibition of prism-face growth and the resulting hexagonal crystals are characteristic of native AFGPs (Figure 4E). Without adsorption to crystalline faces, crystal growth is not predisposed to a specific direction and the structures appear amorphous or round.

Ice shaping data is shown in Figure 4A–D, and full-size images are in the Figures S2–S5. Hexagonal, square, and amorphous crystals were the predominant structures observed, indicating that all of the polymers indeed bind to the surface of specific faces of embryonic ice crystals, resulting in directional growth. Since spicular crystals were not the predominant

https://doi.org/10.1021/acs.biomac.3c01462
Biomacromolecules 2024, 25, 3325−3334

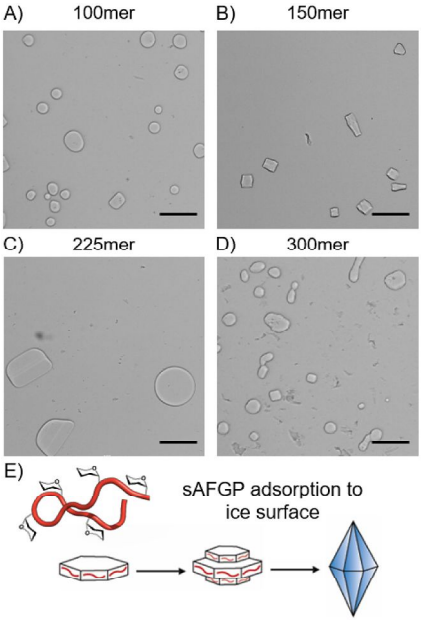

Figure 4. (A–D) Shaping of ice crystals by $(GalHyp_{0.66}\text{-}s\text{-}Ala_{0.33})_n$ glycopolypeptides of varied chain lengths. All samples were prepared at 1 mg/mL in PBS. Scale bars are 100 μm. (E) Cartoon representation of sAFGP adsorbing to ice crystal facing, resulting in shaping of the crystals.

structures observed, the polymers have excellent potential for applications in cryobiology in addition to applications in foods and agriculture.

Polypeptide Conformational Analysis and Mechanistic Discussion. Spectroscopic data indicate native AFGPs adopt an extended structure similar to the left-handed PPII helix. The extended helical structure has been proposed to play a role in the ice-binding mechanism. Therefore, to understand the secondary structures and IRI mechanisms of our various copolypeptides, we conducted analyses using circular dichroism (CD) spectroscopy. This technique relies on the absorption of light by peptide bonds. The wavelengths at which the absorptions occur, and their intensities, reveal characteristics about the orientation of those bonds Distinct CD signatures have been shown for the $\eta \rightarrow \pi^*$ and $\pi \rightarrow \pi^*$ transitions of PPII, intrinsically disordered, sheet, or α-helical conformations.[66−68] In organic solvent, polyPro adopts a compact helical structure with 3.3 residues per turn and cis bonds, termed a PPI helix, while in aqueous solution, the trans-bond PPII structure with 3 residues per turn is favored.[69−75] The PPI vs PPII ratio is affected not only by solvent but also by substituents at the 4-position of the proline ring. The two conformations can be easily differentiated by their absorption ellipticities. The PPI n $\rightarrow \pi^*$ results in a moderate negative minimum at ∼230 nm and a strong maximum at ∼212 nm for $\pi \rightarrow \pi^*$. The PPII form has a minor positive maximum at ∼226 nm and a strong negative minimum at ∼206 nm.

Prior structural work on glycosides of Hyp focused mainly on Hyp-rich glycoproteins that are the major proteinaceous components of higher plant walls, such as Gp1 and extensin.[76,77] Predominant glycan structures are β-galactosides and α-arabinosides with varied chain lengths. CD spectra of these proteins indicated PPII structures; however, the specific effects of glycosylation were unclear since these natural peptides and proteins are typically isolable in only minuscule amounts and/or are heterogeneous in nature.[78] A 2010 study by Owens et al. compared the CD structures of acetyl-capped 9-mers of Pro, Hyp, and β-D-GalHyp.[79] The CD spectra of all three peptides were typical of a PPII helix; however, the glycosylated helices had substantially greater thermal stability. Molecular dynamics simulations indicated that the Gal units interact with both the peptide backbone and one another to result in increased stability. Interestingly, later work by Huang et al. on β-D-GalHyp-containing collagen mimetic peptides reported the glycans slightly destabilized the collagen triple helices, but did not reduce their refolding rate.[80] It should be noted that the interpretation of structural effects in short peptides is convoluted by their small size. Since the PPII helix contains 3 residues per turn, a 9-mer can only form three helical turns.

We obtained CD spectra of our high-molecular-weight GalHyp chains, along with spectra of GalHyp:Pro statistical copolypeptides, so that we could observe any perturbations in structure resulting from increasing glycosylation density (Figure 5A). All data are reported in molar ellipticity, which

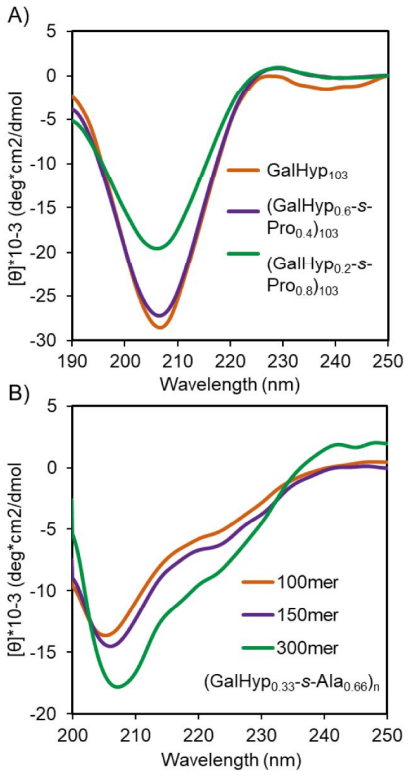

Figure 5. Aqueous circular dichroism data for GalHyp containing polypeptides at 20 °C. Samples were typically prepared at 0.1 mg/mL and data was obtained in Milli-Q water for those in (A) while those in (B) were obtained in PBS buffer.

normalizes for samples of differing concentrations. As expected, all structures revealed spectra characteristic of PPII conformations. Increasing the density of statistically distributed GalHyp from 20% to 60% to 100% resulted in slight increases in characteristic PPII absorbances in the CD spectra, aligning well with prior data *(vide supra)*.

The CD spectra of $(GalHyp_{0.33}\text{-}s\text{-}Ala_{0.66})_n$ were in stark contrast to those of GalHyp and $(GalHyp_x\text{-}s\text{-}Pro_y)_n$ (Figure 5B). The Ala-containing polypeptide spectra are highly characteristic of those of known intrinsically disordered

https://doi.org/10.1021/acs.biomac.3c01462
Biomacromolecules 2024, 25, 3325−3334

peptides.[81,82] This was surprising to us since native AFGPs containing ca. 66% Ala and 33% disaccharide-Thr, and our prior synthetic analogues of identical compositions, adopted PPII-type structures. We also obtained CD spectra at varied temperatures to see if a different conformation is adopted at low temperatures (Figure S1). The spectra at 4 °C were still characteristic of an intrinsically disordered structure, though the absorbances were slightly increased from those at 40 and 80 °C. Ultimately, we can clearly conclude the PPII structure is not required for ice-binding since these disordered structures had high IRI activity.

Considering that the PPII-type structure that is the dominant form of native AFGPs is not required for activity and disordered structures can participate in ice surface interactions, we propose a bulk phenomenon that relies on the entropy of the dehydration of Ala. Computational work previously predicted that Ala is crucial for IRI activity and that the residue's methyl groups nest into ice-surface cavities, driven by the entropy of dehydration.[49] This prediction was corroborated by recent experimental data from our lab that described synthesis of polypeptides with varied Ala content and that sufficiently high Ala content was essential for IRI activity.[41]

This rationale aligns with the data we present here where, despite a prior report on polyPro,[26] polyPro, polyHyp, and poly GalHyp are poor antifreeze materials. Considering the hydrophobicity of polyAla and Ala-rich polypeptides, the hydrophilic sugars are required to both solubilize the material in aqueous solution and likely the solvent-oriented glycan-hydroxyls hydrogen bond to liquid water and prevent ordering of approaching liquid water molecules at the ice surface after the Ala methyls have nested. The higher activity of higher-DP polymers and higher-MW native AFGPs fit with this mechanism since the greater number of Ala groups available on one molecule would offer more stability at the ice surface, overcoming entropic considerations. Interestingly, the optimal effect observed for our polymers was at DP 150, and native AFGPs of highest activity are also ca. 150 residues.[5]

Cytocompatibility Studies. For future biomedical applications, we examined our structures for cytocompatibility. Various similar synthetic glycopolypeptides have been shown by our lab and others to be nontoxic and well tolerated by human cells.[41,83,84] Therefore, we did not expect toxicity or proliferation to be impacted for our sAFGPs. To verify this, we conducted CCK8 assays in human embryonic kidney (HEK) 293 cells. HEK293 cells were selected as a model cell line for broad laboratory use. Viability was measured after 24 h of treatment with sAFGPs of concentrations ranging from 0.2 to 2.0 mg/mL. Cells were treated with PBS as a negative control and Triton X-100 as a positive control (Figure 6). At the highest concentration tested, which exceeded the necessary concentration for IRI activity, no statistically significant effects on cellular viability were observed. Considering that cryogenic applications typically would expose cells to antifreezes at room temperature for only short durations and subfreezing temperatures thereafter, compatibility for 24 h at 37 °C is in excess of likely exposure. From these data, we conclude that these structures are well tolerated by live human cells and are promising for biomedical applications.

CONCLUSIONS

Here, we present a bioinspired synthetic polymer that strongly inhibits the growth of ice crystals. This structure, based on galactosylated hydroxyproline and alanine, is well tolerated by human cells and is composed entirely of natural building blocks. Chain length affected ice recrystallization inhibition activity at a lower molecular weight but plateaued above 150 residues. Natural antifreeze glycoproteins adopt an extended polyproline II-type helical structure. While polymers of galactosylated hydroxyproline adopt this structure, compositions with 66% alanine, as found in native fish antifreeze glycoproteins, were disordered. However, we found that the native conformation is not required for antifreeze activity. Polyproline was previously explored as an antifreeze polymer; however, in our side-by-side comparisons, activity was very poor compared to our structures. Considering the labor and expense required to harvest natural antifreeze glycoproteins, access to efficient synthetics is expected to play important roles in biomedicine, foods, agriculture, coatings, and building materials.

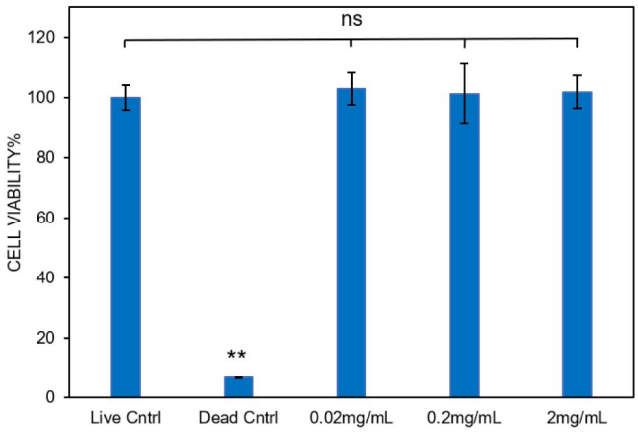

Figure 6. HEK 293 cell viability as determined by CCK8 assay following 24 h incubation with $(GalHyp_{0.66}\text{-}s\text{-}Ala_{0.33})_{150}$ at the indicated concentrations; live control is media alone and Triton X-100 was a positive control for dead cells; standard deviation; ** indicates $p < 0.01$.

ASSOCIATED CONTENT

Supporting Information

The Supporting Information is available free of charge at https://pubs.acs.org/doi/10.1021/acs.biomac.3c01462.

Full experimental details, characterization of compounds, instrumentation, and additional data; representative SEC trace (Figure S1); CD spectra of $(GalHyp_{0.33}\text{-}s\text{-}Ala_{0.66})_{155}$ (Figure S2); $(GalHyp_{0.33}\text{-}s\text{-}Ala_{0.66})_{103}$ (Figure S3), $(GalHyp_{0.33}\text{-}s\text{-}Ala_{0.66})_{155}$ (Figure S4), $(GalHyp_{0.33}\text{-}s\text{-}Ala_{0.66})_{234}$ (Figure S5), and $(GalHyp_{0.33}\text{-}s\text{-}Ala_{0.66})_{312}$ (Figure S6) copolymer full size images of ice shaping; $(Hyp_{0.33}\text{-}s\text{-}Ala_{0.66})_{150}$ ice splat images (Figure S7); IRI images of copolymers (Figures S8, S9); MGS of ice crystals for synthetic polymers (Figure S10); Hyp_{200} ice splat image (Figure S11); Hyp_{200} homopolymer MGS data compared to PBS control (Figure S12); 10% DMSO in PBS ice splat images (Figure S13); $(GalHyp_{0.33}\text{-}s\text{-}Ala_{0.66})_{155}$ ice splat images (Figures S14, S15); $(GalHyp_{0.33}\text{-}s\text{-}Ala_{0.66})_n$ ice splat images (Figure S16); ATR-FTIR (Figures S17, S18); additional polymer data (Table S1) (PDF)

Video showing IRI images of copolymers (MP4)

Video showing IRI images of copolymers (MP4)

https://doi.org/10.1021/acs.biomac.3c01462
Biomacromolecules 2024, 25, 3325−3334

AUTHOR INFORMATION

Corresponding Author

Jessica R. Kramer − *Department of Molecular Pharmaceutics, University of Utah, Salt Lake City, Utah 84112, United States; Department of Biomedical Engineering, University of Utah, Salt Lake City, Utah 84112, United States;* orcid.org/0000-0002-4268-0126; Email: jessica.kramer@utah.edu

Authors

Thomas J. McPartlon − *Department of Molecular Pharmaceutics, University of Utah, Salt Lake City, Utah 84112, United States*

Charles T. Osborne − *Department of Biomedical Engineering, University of Utah, Salt Lake City, Utah 84112, United States*

Complete contact information is available at: https://pubs.acs.org/10.1021/acs.biomac.3c01462

Author Contributions

The manuscript was written through contributions of all authors. All authors have given approval to the final version of the manuscript.

Funding

This work was supported by USA NSF DMR-2300012.

Notes

The authors declare no competing financial interest.

ABBREVIATIONS

NMR,, nuclear magnetic resonance; ATR-FTIR,, attenuated total reflectance Fourier transform infrared spectroscopy; SEC/MALS/RI,, size exclusion chromatography coupled to multiangle light scattering and refractive index detectors; CCK8,, Cell Counting Kit-8; THF,, tetrahydrofuran; MeOH,, methanol

REFERENCES

(1) DeVries, A. L.; Wohlschlag, D. E. Freezing Resistance in Some Antarctic Fishes. *Science* **1969**, *163* (3871), 1073−1075.

(2) Scholander, P. F.; van Dam, L.; Kanwisher, J. W.; Hammel, H. T.; Gordon, M. S. Supercooling and Osmoregulation in Arctic Fish. *J. Cell. Comp. Physiol.* **1957**, *49* (1), 5−24.

(3) Gordon, M. S.; Amdur, B. H.; Scholander, P. F. Freezing Resistance in Some Northern Fishes. *Biol. Bull.* **1962**, *122* (1), 52−62.

(4) Graham, L. A.; Davies, P. L. Glycine-Rich Antifreeze Proteins from Snow Fleas. *Science* **2005**, *310* (5747), 461−461.

(5) Chen, L.; Devries, A. L.; Cheng, C. H. C. Convergent Evolution of Antifreeze Glycoproteins in Antarctic Notothenioid Fish and Arctic Cod. *Proc. Natl. Acad. Sci. U. S. A.* **1997**, *94* (8), 3817−3822.

(6) Budke, C.; Dreyer, A.; Jaeger, J.; Gimpel, K.; Berkemeier, T.; Bonin, A. S.; Nagel, L.; Plattner, C.; Devries, A. L.; Sewald, N.; Koop, T. Quantitative Efficacy Classification of Ice Recrystallization Inhibition Agents. *Cryst. Growth Des.* **2014**, *14* (9), 4285−4294.

(7) Knight, C. A.; De Vries, A. L.; Oolman, L. D. Fish Antifreeze Protein and the Freezing and Recrystallization of Ice. *Nature* **1984**, *308* (5956), 295−296.

(8) Eskandari, A.; Leow, T. C.; Rahman, M. B. A.; Oslan, S. N. Antifreeze Proteins and Their Practical Utilization in Industry, Medicine, and Agriculture. *Biomolecules* **2020**, *10* (12), 1649.

(9) Voets, I. K. From Ice-Binding Proteins to Bio-Inspired Antifreeze Materials. *Soft Mater.* **2017**, *13* (28), 4808−4823.

(10) Bojic, S.; Murray, A.; Bentley, B. L.; Spindler, R.; Pawlik, P.; Cordeiro, J. L.; Bauer, R.; de Magalhães, J. P. Winter is Coming: The Future of Cryopreservation. *BMC Biol.* **2021**, *19* (1), 56.

(11) Brockbank, K. G. M.; Campbell, L. H.; Greene, E. D.; Brockbank, M. C. G.; Duman, J. G. Lessons from Nature for Preservation of Mammalian Cells, Tissues, and Organs. *In Vitro Cell. Dev. Biol.: Anim.* **2011**, *47* (3), 210−217.

(12) Robles, V.; Valcarce, D. G.; Riesco, M. F. The use of Antifreeze Proteins in the Cryopreservation of Gametes and Embryos. *Biomolecules* **2019**, *9* (5), 181.

(13) Amir, G.; Rubinsky, B.; Horowitz, L.; Miller, L.; Leor, J.; Kassif, Y.; Mishaly, D.; Smolinsky, A. K.; Lavee, J. Prolonged 24-h Subzero Preservation of Heterotopically Transplanted Rat Hearts Using Antifreeze Proteins Derived from Arctic Fish. *Ann. Thorac. Surg.* **2004**, *77* (5), 1648−1655.

(14) Meldolesi, A. GM Fish Ice Cream. *Nat. Biotechnol.* **2009**, *27* (8), 682−682.

(15) Best, B. P. Cryoprotectant Toxicity: Facts, Issues, and Questions. *Rejuvenation Res.* **2015**, *18* (5), 422−436.

(16) Verheijen, M.; Lienhard, M.; Schrooders, Y.; Clayton, O.; Nudischer, R.; Boerno, S.; Timmermann, B.; Selevsek, N.; Schlapbach, R.; Gmuender, H.; et al. DMSO Induces Drastic Changes in Human Cellular Processes and Epigenetic Landscape in Vitro. *Sci. Rep.* **2019**, *9* (1), 4641.

(17) Ekpo, M. D.; Tan, S.; Xie, J.; Hu, Y.; Liu, X.; Liu, F.; Xiang, J.; Zhao, R.; Wang, B. Antifreeze Proteins: Novel Applications and Navigation towards Their Clinical Application in Cryobanking. *Int. J. Mol. Sci.* **2022**, *23* (5), 2639.

(18) Liu, Z.; Zheng, X.; Wang, J. Bioinspired Ice-Binding Materials for Tissue and Organ Cryopreservation. *J. Am. Chem. Soc.* **2022**, *144* (13), 5685−5701.

(19) Mitchell, D. E.; Cameron, N. R.; Gibson, M. I. Rational, yet Simple, Design and Synthesis of an Antifreeze-Protein Inspired Polymer for Cellular Cryopreservation. *Chem. Commun.* **2015**, *51* (65), 12977−12980.

(20) Eniade, A.; Ben, R. N. Fully Convergent Solid Phase Synthesis of Antifreeze Glycoprotein Analogues. *Biomacromolecules* **2001**, *2* (2), 557−561.

(21) Wilkinson, B. L.; Stone, R. S.; Capicciotti, C. J.; Thaysen-Andersen, M.; Matthews, J. M.; Packer, N. H.; Ben, R. N.; Payne, R. J. Total Synthesis of Homogeneous Antifreeze Glycopeptides and Glycoproteins. *Angew. Chem., Int. Ed.* **2012**, *51* (15), 3606−3610.

(22) Eniade, A.; Murphy, A. V.; Landreau, G.; Ben, R. N. A General Synthesis of Structurally Diverse Building Blocks for Preparing Analogues of C-Linked Antifreeze Glycoproteins. *Bioconjugate Chem.* **2001**, *12* (5), 817−823.

(23) Tseng, P. H.; Jiaang, W. T.; Chang, M. Y.; Chen, S. T. Facile Solid-Phase Synthesis of an Antifreeze Glycoprotein. *Chem. - Eur. J.* **2001**, *7* (3), 585−590.

(24) Urbaäczyk, M.; Góra, J.; Latajka, R.; Sewald, N. Antifreeze Glycopeptides: From Structure and Activity Studies to Current Approaches in Chemical Synthesis. *Amino Acids* **2017**, *49* (2), 209−222.

(25) Deller, R. C.; Vatish, M.; Mitchell, D. A.; Gibson, M. I. Synthetic Polymers Enable Non-Vitreous Cellular Cryopreservation by Reducing Ice Crystal Growth during Thawing. *Nat. Commun.* **2014**, *5*, 3244.

(26) Judge, N.; Georgiou, P. G.; Bissoyi, A.; Ahmad, A.; Heise, A.; Gibson, M. I. High Molecular Weight Polyproline as a Potential Biosourced Ice Growth Inhibitor: Synthesis, Ice Recrystallization Inhibition, and Specific Ice Face Binding. *Biomacromolecules* **2023**, *24* (6), 2459−2468.

(27) Geng, H.; Liu, X.; Shi, G.; Bai, G.; Ma, J.; Chen, J.; Wu, Z.; Song, Y.; Fang, H.; Wang, J. Graphene Oxide Restricts Growth and Recrystallization of Ice Crystals. *Angew. Chem., Int. Ed.* **2017**, *56* (4), 997−1001.

(28) Qin, Q.; Zhao, L.; Liu, Z.; Liu, T.; Qu, J.; Zhang, X.; Li, R.; Yan, L.; Yan, J.; Jin, S.; et al. Bioinspired l -Proline Oligomers for the Cryopreservation of Oocytes via Controlling Ice Growth. *ACS Appl. Mater. Interfaces* **2020**, *12* (16), 18352−18362.

(29) Jin, S.; Yin, L.; Kong, B.; Wu, S.; He, Z.; Xue, H.; Liu, Z.; Cheng, Q.; Zhou, X.; Wang, J. Spreading Fully at the Ice-Water

Interface is Required for High Ice Recrystallization Inhibition Activity. *Sci. China: Chem.* **2019**, *62* (7), 909−915.
(30) Graham, B.; Bailey, T. L.; Healey, J. R. J.; Marcellini, M.; Deville, S.; Gibson, M. I. Polyproline as a Minimal Antifreeze Protein Mimic that Enhances the Cryopreservation of Cell Monolayers. *Angew. Chem., Int. Ed.* **2017**, *56* (50), 15941−15944.
(31) Ben, R. N.; Eniade, A. A.; Hauer, L. Synthesis of a C-Linked Antifreeze Glycoprotein (AFGP) Mimic: Probes for Investigating the Mechanism of Action. *Org. Lett.* **1999**, *1* (11), 1759−1762.
(32) Liu, S.; Ben, R. N. C-Linked Galactosyl Serine AFGP Analogues as Potent Recrystallization Inhibitors. *Org. Lett.* **2005**, *7* (12), 2385−2388.
(33) Tsuda, T.; Nishimura, S. I. Synthesis of an Antifreeze Glycoprotein Analogue: Efficient Preparation of Sequential Glycopeptide Polymers. *Chem. Commun.* **1996**, No. 24, 2779−2780.
(34) Huang, M. L.; Ehre, D.; Jiang, Q.; Hu, C.; Kirshenbaum, K.; Ward, M. D. Biomimetic Peptoid Oligomers as Dual-Action Antifreeze Agents. *Proc. Natl. Acad. Sci. U. S. A.* **2012**, *109* (49), 19922−19927.
(35) Filira, F.; Biondi, L.; Scolaro, B.; Foffani, M. T.; Mammi, S.; Peggion, E.; Rocchi, R. Solid Phase Synthesis and Conformation of Sequential Glycosylated Polytripeptide Sequences Related to Antifreeze Glycoproteins. *Int. J. Biol. Macromol.* **1990**, *12* (1), 41−49.
(36) Tachibana, Y.; Fletcher, G. L.; Fujitani, N.; Tsuda, S.; Monde, K.; Nishimura, S. I. Antifreeze Glycoproteins: Elucidation of the Structural Motifs that are Essential for Antifreeze Activity. *Angew. Chem., Int. Ed.* **2004**, *43* (7), 856−862.
(37) Tachibana, Y.; Matsubara, N.; Nakajima, F.; Tsuda, T.; Tsuda, S.; Monde, K.; Nishimura, S. I. Efficient and Versatile Synthesis of Mucin-like Glycoprotein Mimics. *Tetrahedron* **2002**, *58* (51), 10213−10224.
(38) Sun, Y.; Maltseva, D.; Liu, J.; Hooker, T.; Mailänder, V.; Ramløv, H.; Devries, A. L.; Bonn, M.; Meister, K. Ice Recrystallization Inhibition is Insufficient to Explain Cryopreservation Abilities of Antifreeze Proteins. *Biomacromolecules* **2022**, *23* (3), 1214−1220.
(39) Bailey, T. L.; Graham, B.; Stubbs, C.; Gibson, M. I. Bio-Inspired Cryopreservation Using Synthetic Polymer Analogues. *Cryobiology* **2018**, *85*, 129.
(40) Phillips, D. J.; Congdon, T. R.; Gibson, M. I. Activation of Ice Recrystallization Inhibition Activity of Poly(Vinyl Alcohol) Using a Supramolecular Trigger. *Polym. Chem.* **2016**, *7* (9), 1701−1704.
(41) Deleray, A. C.; Saini, S. S.; Wallberg, A. C.; Kramer, J. R. Synthetic Antifreeze Glycoproteins with Potent Ice-Binding Activity. *Chem. Mater.* **2024**, *36* (7), 3424−3434.
(42) DeVries, A. L.; Komatsu, S. K.; Feeney, R. E. Chemical and Physical Properties of Freezing Point-Depressing Glycoproteins from Antarctic Fishes. *J. Biol. Chem.* **1970**, *245* (11), 2901−2908.
(43) Raymond, J. A.; Radding, W.; DeVries, A. L. Circular Dichroism of Protein and Glycoprotein Fish Antifreezes. *Biopolymers* **1977**, *16* (11), 2575−2578.
(44) Franks, F.; Morris, E. R. Blood Glycoprotein from Antarctic Fish Possible Conformational Origin of Antifreeze Activity. *Biochim. Biophys. Acta, Gen. Subj.* **1978**, *540* (2), 346−356.
(45) Deleray, A. C.; Kramer, J. R. Biomimetic Glycosylated Polythreonines by N-Carboxyanhydride Polymerization. *Biomacromolecules* **2022**, *23* (3), 1453−1461.
(46) Raymond, J. A.; DeVries, A. L. Adsorption Inhibition as a Mechanism of Freezing Resistance in Polar Fishes. *Proc. Natl. Acad. Sci. U. S. A.* **1977**, *74* (6), 2589−2593.
(47) Liu, K.; Wang, C.; Ma, J.; Shi, G.; Yao, X.; Fang, H.; Song, Y.; Wang, J. Janus Effect of Antifreeze Proteins on Ice Nucleation. *Proc. Natl. Acad. Sci. U. S. A.* **2016**, *113* (51), 14739−14744.
(48) Ben, R. N. Antifreeze Glycoproteins - Preventing the Growth of Ice. *ChemBiochem* **2001**, *2* (3), 161−166.
(49) Mochizuki, K.; Molinero, V. Antifreeze Glycoproteins Bind Reversibly to Ice via Hydrophobic Groups. *J. Am. Chem. Soc.* **2018**, *140* (14), 4803−4811.
(50) Pandey, P.; Mallajosyula, S. S. Elucidating the Role of Key Structural Motifs in Antifreeze Glycoproteins. *Phys. Chem. Chem. Phys.* **2019**, *21* (7), 3903−3917.
(51) Ebbinghaus, S.; Meister, K.; Born, B.; Devries, A. L.; Gruebele, M.; Havenith, M. Antifreeze Glycoprotein Activity Correlates with Long-Range Protein-Water Dynamics. *J. Am. Chem. Soc.* **2010**, *132* (35), 12210−12211.
(52) Meister, K.; Devries, A. L.; Bakker, H. J.; Drori, R. Antifreeze Glycoproteins Bind Irreversibly to Ice. *J. Am. Chem. Soc.* **2018**, *140* (30), 9365−9368.
(53) Tsuda, S.; Yamauchi, A.; Uddin Khan, N. M. M.; Arai, T.; Mahatabuddin, S.; Miura, A.; Kondo, H. Fish-Derived Antifreeze Proteins and Antifreeze Glycoprotein Exhibit a Different Ice-Binding Property with Increasing Concentration. *Biomolecules* **2020**, *10* (3), 423.
(54) Berger, T.; Meister, K.; Devries, A. L.; Eves, R.; Davies, P. L.; Drori, R. Synergy between Antifreeze Proteins is Driven by Complementary Ice-Binding. *J. Am. Chem. Soc.* **2019**, *141* (48), 19144−19150.
(55) Biggs, C. I.; Bailey, T. L.; Graham, B.; Stubbs, C.; Fayter, A.; Gibson, M. I. Polymer Mimics of Biomacromolecular Antifreezes. *Nat. Commun.* **2017**, *8* (1), 1546.
(56) Detwiler, R. E.; Schlirf, A. E.; Kramer, J. R. Rethinking Transition Metal Catalyzed N-Carboxyanhydride Polymerization: Polymerization of Pro and AcOPro N-Carboxyanhydrides. *J. Am. Chem. Soc.* **2021**, *143* (30), 11482−11489.
(57) Kramer, J. R.; Deming, T. J. General Method for Purification of α-Amino Acid-N-Carboxyanhydrides Using Flash Chromatography. *Biomacromolecules* **2010**, *11* (12), 3668−3672.
(58) Deming, T. J. Cobalt and Iron Initiators for the Controlled Polymerization of α-Amino Acid-N-Carboxyanhydrides. *Macromolecules* **1999**, *32* (13), 4500−4502.
(59) Detwiler, R. E.; McPartlon, T. J.; Coffey, C. S.; Kramer, J. R. Clickable Polyprolines from Azido-Proline N -Carboxyanhydride. *ACS Polym. Au* **2023**, *3* (5), 383−393.
(60) Brzezinska, K. R.; Curtin, S. A.; Deming, T. J. Polypeptide End-Capping Using Functionalized Isocyanates: Preparation of Pentablock Copolymers. *Macromolecules* **2002**, *35* (8), 2970−2976.
(61) Kramer, J. R.; Onoa, B.; Bustamante, C.; Bertozzi, C. R. Chemically Tunable Mucin Chimeras Assembled on Living Cells. *Proc. Natl. Acad. Sci. U. S. A.* **2015**, *112* (41), 12574−12579.
(62) Biggs, C. I.; Stubbs, C.; Graham, B.; Fayter, A. E. R.; Hasan, M.; Gibson, M. I. Mimicking the Ice Recrystallization Activity of Biological Antifreezes. When is a New Polymer "Active"? *Macromol. Biosci.* **2019**, *19* (7), 1900082.
(63) Campos-García, V. R.; Herrera-Fernández, D.; Espinosa-De La Garza, C. E.; González, G.; Vallejo-Castillo, L.; Avila, S.; Muñoz-García, L.; Medina-Rivero, E.; Pérez, N. O.; Gracia-Mora, I.; et al. Process Signatures in Glatiramer Acetate Synthesis: Structural and Functional Relationships. *Sci. Rep.* **2017**, *7* (1), 1−12.
(64) DeVries, A. L. Glycoproteins as Biological Antifreeze Agents in Antarctic Fishes. *Science* **1971**, *172* (3988), 1152−1155.
(65) DeVries, A. L. Antifreeze Glycopeptides and Peptides: Interactions with Ice and Water. *Methods Enzymol.* **1986**, *127* (C), 293−303.
(66) Greenfield, N. J. Using Circular Dichroism Spectra to Estimate Protein Secondary Structure. *Nat. Protoc.* **2006**, *1* (6), 2876−2890.
(67) Kelly, S. M. M. M.; Price, N. C. C. C. The Use of Circular Dichroism in the Investigation of Protein Structure and Function. *Curr. Protein Pept. Sci.* **2000**, *1* (4), 349−384.
(68) van Stokkum, I. H.; Spoelder, H. J.; Bloemendal, M.; van Grondelle, R.; Groen, F. C. Estimation of Protein Secondary Structure and Error Analysis from Circular Dichroism Spectra. *Anal. Biochem.* **1990**, *191* (1), 110−118.
(69) Traub, W.; Shmueli, U. Structure of Poly-L-Proline I. *Nature* **1963**, *198* (4886), 1165−1166.
(70) Cowan, P. M.; McGavin, S.; North, A. C. The Polypeptide Chain Configuration of Collagen. *Nature* **1955**, *176*, 1062−1064.

https://doi.org/10.1021/acs.biomac.3c01462
Biomacromolecules 2024, 25, 3325−3334

(71) Steinberg, I. Z.; Harrington, W. F.; Berger, A.; Sela, M.; Katchalski, E. The Configurational Changes of Poly-L-Proline in Solution. *J. Am. Chem. Soc.* **1960**, *82* (20), 5263−5279.
(72) Harrington, W. F.; Sela, M. Studies on the Structure of Poly-l-Proline in Solution. *Biochim. Biophys. Acta* **1958**, *27*, 24−41.
(73) Kurtz, J.; Berger, A.; Katchalski, E. Mutarotation of Poly-L-Proline. *Nature* **1956**, *178*, 1066−1067.
(74) Steinberg, I. Z.; Berger, A.; Katchalski, E. Reverse Mutarotation of Poly-l-Proline. *Biochim. Biophys. Acta* **1958**, *28*, 647−648.
(75) Dukor, R. K.; Keiderling, T. A. Mutarotation Studies of Poly-L-Proline Using FTIR, Electronic and Vibrational Circular Dichroism. *Biospectroscopy* **1996**, *2* (2), 83−100.
(76) Ferris, P. J.; Woessner, J. P.; Waffenschmidt, S.; Kilz, S.; Drees, J.; Goodenough, U. W. Glycosylated Polyproline II Rods with Kinks as a Structural Motif in Plant Hydroxyproline-Rich Glycoproteins. *Biochemistry* **2001**, *40* (9), 2978−2987.
(77) Liang, R.; You, L.; Dong, F.; Zhao, X.; Zhao, J. Identification of Hydroxyproline-Containing Proteins and Hydroxylation of Proline Residues in Rice. *Front. Plant Sci.* **2020**, *11*, 1207.
(78) Taylor, C. M.; Karunaratne, C. V.; Xie, N. Glycosides of Hydroxyproline: Some Recent, Unusual Discoveries. *Glycobiology* **2012**, *22* (6), 757−767.
(79) Owens, N. W.; Stetefeld, J.; Lattovaì, E.; Schweizer, F. Contiguous O -Galactosylation of 4(R)-Hydroxy- l -Proline Residues Forms Very Stable Polyproline II Helices. *J. Am. Chem. Soc.* **2010**, *132* (14), 5036−5042.
(80) Huang, P. W.; Chang, J. M.; Horng, J. C. Effects of Glycosylated (2S,4R)-Hydroxyproline on the Stability and Assembly of Collagen Triple Helices. *Amino Acids* **2016**, *48* (12), 2765−2772.
(81) Miles, A. J.; Drew, E. D.; Wallace, B. A. DichroIDP: A Method for Analyses of Intrinsically Disordered Proteins Using Circular Dichroism Spectroscopy. *Commun. Biol.* **2023**, *6* (1), 823.
(82) Chemes, L. B.; Alonso, L. G.; Noval, M. G.; De Prat-Gay, G. Circular Dichroism Techniques for the Analysis of Intrinsically Disordered Proteins and Domains. *Methods Mol. Biol.* **2012**, *895*, 387−404.
(83) Wardzala, C. L.; Clauss, Z. S.; Kramer, J. R. Principles of Glycocalyx Engineering with Hydrophobic-Anchored Synthetic Mucins. *Front. Cell Dev. Biol.* **2022**, *10*, 1−13.
(84) Kohout, V. R.; Wardzala, C. L.; Kramer, J. R. Mirror Image Mucins and Thio Mucins with Tunable Biodegradation. *J. Am. Chem. Soc.* **2023**, *145* (30), 16573−16583.

https://doi.org/10.1021/acs.biomac.3c01462
Biomacromolecules 2024, 25, 3325−3334